

PDF hosted at the Radboud Repository of the Radboud University Nijmegen

The following full text is a publisher's version.

For additional information about this publication click this link.

<http://hdl.handle.net/2066/99002>

Please be advised that this information was generated on 2019-06-16 and may be subject to change.

High Rydberg states of DABCO: Spectroscopy, ionization potential, and comparison with mass analyzed threshold ionization

Maarten G. H. Boogaarts, Iwan Holleman, Rienk T. Jongma, David H. Parker, and Gerard Meijer

Department of Molecular and Laser Physics, Catholic University of Nijmegen, Toernooiveld 1, NL-6525 ED Nijmegen, The Netherlands

Uzi Even

Sackler Faculty of Exact Sciences, Department of Chemistry, Tel Aviv University, 69978 Tel Aviv, Israel

(Received 8 August 1995; accepted 6 December 1995)

Doubly-resonant excitation/vibrational autoionization is used to accurately determine the ionization potential (IP) of the highly symmetric caged amine 1,4 diazabicyclo[2,2,2]octane (DABCO). The IP of DABCO excited with one quantum of the $\nu_{24}(e')$ vibration lies at $(59\,048.62 \pm 0.03) \text{ cm}^{-1}$, based on fitting 56 components of the np_{xy} Rydberg series ($\delta = 0.406 \pm 0.002$) to the Rydberg formula. Rydberg state transition energies and linewidths are determined using standard calibration and linefitting techniques. The IP determined from Rydberg state extrapolation is compared with that determined by mass analyzed threshold ionization (MATI). Effects of static electric fields on MATI signals measured for the high Rydberg states are discussed. © 1996 American Institute of Physics. [S0021-9606(96)04310-8]

I. INTRODUCTION

Highly excited molecular Rydberg states have become an increasingly interesting research field, in part due to development of zero kinetic energy (ZEKE) photoelectron spectroscopy by Müller-Dethlefs and Schlag,¹ and of the mass-selective variant mass analyzed threshold ionization (MATI) by Johnson and co-workers.² Both techniques can yield high-resolution spectra³ of molecular ions by detecting precursor molecular Rydberg states through pulsed field ionization. The unexpected stability of these molecular Rydberg states as seen in ZEKE and MATI experiments^{4,5,6} has led to a number of different models,^{7,8,9} guided by the extensive work on atomic Rydberg states¹⁰ and on simple diatomic systems.¹¹⁻¹⁴ Highly excited molecular Rydberg states of larger polyatomics have also been studied¹⁵⁻¹⁹ but very few molecules show resolvable Rydberg progressions with principal quantum numbers $n > 50$, which are the states probed by ZEKE/MATI. The highly symmetric caged amine DABCO (see Fig. 1) is an exception,²⁰ and states with n up to 80 are observed here.

One goal of this study is to compare the DABCO IP measured using Rydberg state extrapolation with that derived by the MATI method. Previous comparisons, for example, for benzene¹⁸ and ammonia¹⁹ show disagreements which could possibly lie in the calibration of either technique. Efforts are made to increase the accuracy by detection of higher Rydberg levels and by improving the calibration of the transition wavelengths. Transition linewidths are also more accurately determined in light of the remarkable differences found previously²⁰ between Rydberg state lifetimes implied from linewidths and from ZEKE time delays. Furthermore, the effects of applied fields and time delays between excitation and pulsed field ionization on the observed Rydberg spectra are followed. Strong effects on the Rydberg spectra

due to the small bias fields in the MATI experiment are also observed.

Rydberg states of DABCO have been the subject of a number of double resonance ionization studies,^{15,21-24} the most extensive being those of Ito and co-workers.¹⁵ Our study follows the recent work of Even and co-workers²⁰ where ZEKE and double-resonance autoionization were compared. Our results are in good agreement with the previous studies but focus on more accurate energy calibrations and on higher Rydberg levels where the effects of applied static fields are most observable.

A. Energy levels and ionization pathways

Relevant energy levels and ionization pathways for this study are given schematically in Fig. 1. The first electronically excited state of DABCO results from excitation of a lone pair electron $n(+)(a'_1)$ to a $3s$ Rydberg orbital (a'_1). This ${}^1A'_1 \leftarrow {}^1A'_1$ transition is one-photon forbidden in D_{3h} symmetry but gains intensity through vibronic coupling with the nearby $3p_{xy}$ Rydberg state (${}^1E'$, $39\,830 \text{ cm}^{-1}$). One-photon excitation at 271.78 nm is thereby possible to the $\nu_{24}(e')$ mode (1011.27 cm^{-1}). This transition is chosen because it is one of the strongest in the one-photon spectrum and because it lies at a convenient dye laser wavelength. The electronically excited states of DABCO are all Rydberg in nature²⁵ and the ground state absorption spectrum is dominated by the np_{xy} Rydberg series. The strongest Rydberg series studied here, arising from the $3s$ Rydberg intermediate state, belong also to the np_{xy} series.²³ Weaker Rydberg series due to ns and nd orbital excitation¹⁵ seen also in the spectra shown later are not analyzed in this study.

Vibrational autoionization ($\Delta v = -1$) can take place from vibrationally excited (e') Rydberg levels lying above the vibrationless IP_0 .¹⁵ In our experiment, levels with $n \geq 11$ converging to the ν_{24} level of the ion autoionize. Processes

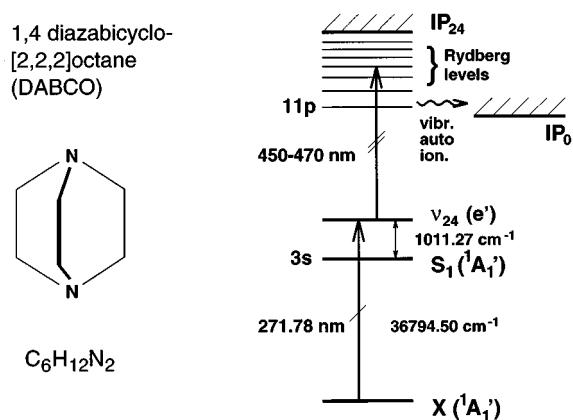


FIG. 1. Structure of 1,4 diazabicyclo[2,2,2]octane (DABCO) and the energy levels that are used in this study. See the text for a detailed description.

such as l and m_l state mixing due to stray fields,⁷ collisions,²⁶ or the presence of ions⁹ can stabilize and/or destabilize the higher Rydberg levels against autoionization. The stable states in our study are detected 6 μ s after excitation by pulsed field ionization (PFI).

II. EXPERIMENT

A standard pulsed beam laser ionization mass spectrometer²⁷ with mutually perpendicular molecular beam, laser beam(s), and linear time-of-flight axes is employed. DABCO vapor at 40 °C is seeded into a pulsed beam expansion of Ne which is skimmed before entering the ionization region. Previous studies²⁸ indicate a DABCO rotational temperature of 2 K, and the absence of any interfering clusters²⁹ for the present beam conditions.

Tunable counterpropagating pulsed (5 ns pulse length) beams from two dye lasers, pumped by separate Nd:YAG lasers are used to first excite DABCO from the vibrationless ground state to the ν_{24} vibrational level of the $A'(3s)$ state followed by a second excitation step to the high Rydberg levels. The first (preparation) laser beam is frequency doubled in a KDP crystal and tuned to the maximum of the $A\ 24_0^1 \leftarrow X$ transition at 271.78 nm.²⁸ This laser has a pulse energy of 0.5 mJ and a linewidth of 0.5 cm^{-1} , which excites a range of J, K states up to $J=K=5$.²⁸ Special calibration of the preparation laser was not necessary since the origin of the transition is already known to high accuracy ($36\ 794.501 \pm 0.007\text{ cm}^{-1}$).²⁸

The laser used for excitation to the high Rydberg states is tunable in the 450–470 nm region (coumarin 460 dye pumped by 355 nm) with a linewidth of 0.08 cm^{-1} . Minimal pulse energies (always less than 2 mJ) consistent with an acceptable signal to noise were used to avoid resonant two-photon ionization and to minimize power broadening, which has been observed for the low Rydberg states ($n \leq 30$). Calibration of the excitation laser was done by simultaneously measuring the absorption spectra of $^{130}\text{Te}_2$ in an oven oper-

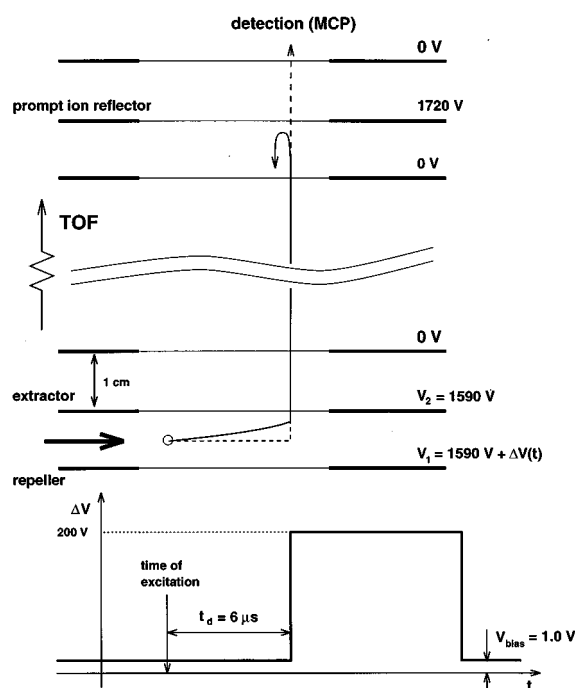


FIG. 2. Schematic representation of the ion-optics and the time-dependent extraction fields used in this experiment. Prompt ions as well as Rydberg neutrals are produced between the extraction plates of a linear time-of-flight mass spectrometer at the position indicated by the circle. After a time-delay of typically 6 μ s an extraction pulse is applied to field ionize the Rydberg neutrals and to accelerate the ions toward the detector. Both the trajectories of the prompt ions (solid curve) and of the (field-ionized) Rydberg neutrals (dashed curve) are indicated.

ated at 450 °C. Abundant absorption lines, tabulated to high accuracy ($\pm 0.001\text{ cm}^{-1}$) (Ref. 30) are available for $^{130}\text{Te}_2$ in this energy region.

Figure 2 is a schematic diagram of the ion optics and pulse sequences used in the linear time-of-flight mass spectrometer. Ions are formed between the repeller and extractor plates (52 mm circular electrodes with a 15 mm diam 75% transparent honeycomb mesh) and accelerated to the front grid of a time-of-flight (TOF) mass spectrometer tube held at earth potential. The extractor plate is held constant at 1590 V while the repeller is pulsed from 1590 V (effective zero-field) to more positive potentials.

Two different types of measurements are carried out; integrated double-resonance where all ions are collected, and MATI, which selectively detects ions formed by pulsed-field ionization (PFI) from only the highest excited Rydberg states. In the integrated double-resonance measurement the Rydberg states are initially excited in a zero-applied field ($V_{\text{bias}}=0\text{ V}$, assuming stray electric fields $<100\text{ mV/cm}$) and then 4 μ s after laser excitation of the Rydberg states a 200 V/cm pulse is applied to the repeller plate. Combined with a permanent acceleration voltage on the extractor this 200 V pulse ensures Wiley–McLaren space-focusing with a mass resolution of 400 for the 60 cm long TOF tube. Ions that are collected can be formed by several different processes: direct 1-color 2-photon ionization or 2-color (1+2)-photon ioniza-

tion, vibrational autoionization, and pulsed field ionization (PFI).

A variety of experimental approaches to enable selective detection of long-lived high Rydberg states in a MATI-experiment have been demonstrated.^{2,27,31–34} Here the experimental difference between the “integrated double-resonance” measurements and the MATI measurements is the application in the latter case of a small electric bias field in the extraction region, and a high voltage on an ion reflector in front of the detector. The bias field (between 0.5 and 4 V/cm) is present either before or shortly (<100 ns) after the excitation laser pulse arrives. This bias field causes all ions to slowly drift upwards, apart from the neutral molecules. After a long pause (typically 6 μ s) the 200 V/cm pulse is applied. With time delays longer than 10 μ s the excited molecules, traveling with the velocity of the Ne-beam, leave the collection region of the ion optics.

Owing to their vertical displacement, the ions formed before the application of the 200 V/cm pulse experience a lower potential and thus obtain a lower kinetic energy than the ions formed by PFI at 200 V. The lower kinetic energy ions are selectively blocked by the reflector field of an electrode at the end of the time-of-flight tube. This blocking is accomplished by setting the bias field to 0.5 V/cm and the time delay between laser excitation and pulsed field ionization/extraction to typically 6 μ s. The Rydberg excitation laser is then set in frequency to ≈ 5 cm^{-1} above the ionization threshold. Then the reflector voltage is increased until the DABCO ion peak has completely vanished, effectively blocking all prompt ions formed by the excitation laser above (or below) the IP. Ions formed by pulsed field ionization of Rydberg states can still reach the detector under these conditions. The reflector voltage effectively determines a region between repeller and extractor plates from which ions present in this region at the time of the extraction pulse can reach the detector. The size of this region is set in these experiments to be the same in all MATI measurements, i.e., independent of the value of the bias field. The reflector is set to a potential of 1720 V which corresponds to a window size of 3.5 mm measured from the repeller plate.

Müller-Dethlefs and co-workers³ have shown that there are two advantages to pulsing the bias field on after the laser pulse in the MATI experiment. First, a much stronger signal is found due to the presence of more highly excited Rydberg states in the “magic” region very near the IP which contribute most to the MATI signal,¹ and second, the absence of (small) static electric fields during excitation prevents undesired field effects on the Rydberg state spectra.^{36–39}

At the end of the TOF tube the ions corresponding to the DABCO mass are collected and amplified by a dual micro-channelplate detector which is connected to a 10 bit digital oscilloscope/computer. A separate channel of the digital scope is used to monitor simultaneously the transmission of the excitation laser through the ¹³⁰Te₂ cell. The computer also controls the Rydberg excitation laser wavelength scans. Fitting of the observed spectral lineshapes is carried out with standard line-fitting routines.

III. RESULTS AND ANALYSIS

A. Ionization potential, quantum defect, and linewidths

The IP of DABCO excited with one quantum of ν_{24} is determined by fitting the measured energy positions of the observed np_{xy} Rydberg series to the formula $E_n = \text{IP} - R_{\text{dabco}}/(n - \delta)^2$, where E_n is the measured transition energy for principle quantum number n , R_{dabco} is the reduced-mass corrected Rydberg constant (109 736.777 cm^{-1}), and δ is the quantum defect. Table I lists the observed energy positions with their uncertainties plus the deviation of each line from the calculated value. The energy positions were determined by first fitting each line with a Lorentzian profile and taking the transition energy as the center of the fit Lorentzian. Although n values up to $n=79$ were observed, only levels up to $n=66$ were fit due to signal to noise limitations. Most of the lines could be reasonably fit with the Lorentzian shape and no strongly Fano-type profiles¹⁵ were seen in this work. Some of the lines, especially those corresponding to intensity dips (vide infra), could possibly be better fit with a non-Lorentzian line shape. Figure 3 shows a part of the np_{xy} Rydberg series with principal quantum numbers $19 \leq n \leq 32$. The other lines in this figure can be attributed to other δ -series¹⁵ and are not analyzed in this study. The figure shows separately the $n=19$ and the $n=32$ Rydberg lines together with their fitted Lorentzian profiles.

The fit accurately determines the values for the (adiabatic) ionization potential and quantum defect to be $\text{IP} = (22\,254.121 \pm 0.023) \text{ cm}^{-1}$ and $\delta = (0.4062 \pm 0.0021)$, respectively. The stated errors are three times the standard deviations calculated from the fit. Adding $(36\,794.501 \pm 0.007) \text{ cm}^{-1}$ for the transition energy of the preparation step gives for the energy of the vibrational level in the ion $(59\,048.622 \pm 0.024) \text{ cm}^{-1}$.

Rydberg line positions were also fit with a n -dependent quantum defect δ_n where δ_n is related to the energy of the state via $\delta_n = \delta + \epsilon(\text{IP} - E_n) \approx \delta + \epsilon R/(n - \delta)^2$, and where ϵ represents a distortion parameter. This yields a slight improvement of the quality of the fit (standard deviation of the fit decreases from 0.050 cm^{-1} to 0.047 cm^{-1}) and the values for the fit parameters are in this case $\text{IP} = (22\,254.109 \pm 0.026) \text{ cm}^{-1}$, $\delta = (0.4024 \pm 0.0051)$, and $\epsilon = (5.2 \pm 2.1) \times 10^{-6} / \text{cm}^{-1}$ [or $\epsilon R = (0.57 \pm 0.23)$].

With the fitted value for the IP the quantum defect can be calculated for each line from the observed line position. The result is shown in Fig. 4. In this figure the quantum defect (with its error) is plotted as a function of the energy of the Rydberg states. Also shown in this figure are the (constant) quantum defect determined from the first fit (solid line), and the functional form of the n -dependent quantum defect as determined from the second fit (dashed line). It is evident that the value for the quantum defect is mainly determined by the Rydberg states with low n value and the figure shows that there is no significant difference between the two fits in this region.

Table I also lists the linewidths of the Rydberg states. From Fig. 3 it can also be seen that this linewidth decreases

TABLE I. Line positions of Rydberg states of 1,4 diazabicyclo[2,2,2]octane (DABCO) with principal quantum numbers $11 \leq n \leq 66$. The line positions have been fitted with a least-squares fitting algorithm to the Rydberg formula, $E_n = \text{IP} - R/(n - \delta)^2$. For each Rydberg state are given the observed line position with experimental error, the difference with the line position calculated from the fit, and the width of the Rydberg line with error, respectively, all in wave numbers. The given values are for the excitation laser only. The line positions have been calibrated against the $^{130}\text{Te}_2$ absorption spectrum. From the fit the values for the ionization potential and the quantum defect are determined to be $\text{IP} = (22\,254,121 \pm 0.023) \text{ cm}^{-1}$ and $\delta = (0.4062 \pm 0.0021)$, respectively.

n	Observed	(Error)	Obs-calc	Width	(Error)	n	Observed	(Error)	Obs-calc	Width	(Error)
11	21 276.30	(0.20)	-0.03	2.0	(0.5)	39	22 180.42	(0.06)	-0.02	0.35	(0.05)
12	21 436.97	(0.40)	-0.76	2.4	(0.1)	40	22 184.10	(0.06)	-0.02	0.30	(0.05)
13	21 561.80	(0.40)	-0.43	3.0	(0.5)	41	22 187.55	(0.04)	0.02	0.38	(0.05)
14	21 659.70	(0.40)	-0.58	2.9	(0.5)	42	22 190.69	(0.06)	0.00	0.29	(0.05)
15	21 739.13	(0.40)	0.26	2.3	(0.5)	43	22 193.63	(0.06)	-0.00	0.26	(0.05)
16	21 802.95	(0.15)	0.11	1.3	(0.5)	44	22 196.38	(0.06)	0.00	0.27	(0.05)
17	21 855.58	(0.15)	-0.01	1.5	(0.5)	45	22 198.98	(0.06)	0.04	0.27	(0.05)
18	21 899.37	(0.20)	-0.24	1.4	(0.4)	46	22 201.35	(0.06)	0.02	0.19	(0.05)
19	21 936.40	(0.15)	-0.31	1.3	(0.3)	47	22 203.57	(0.04)	-0.00	0.24	(0.05)
20	21 968.30	(0.20)	-0.01	1.4	(0.5)	48	22 205.69	(0.06)	0.02	0.22	(0.05)
21	21 995.17	(0.25)	-0.20	1.6	(0.3)	49	22 207.65	(0.06)	0.00	0.23	(0.05)
22	22 019.09	(0.30)	0.31	1.8	(0.3)	50	22 209.51	(0.06)	0.01	0.26	(0.05)
23	22 039.30	(0.15)	0.15	1.0	(0.1)	51	22 211.23	(0.04)	-0.02	0.21	(0.05)
24	22 057.25	(0.15)	0.26	0.7	(0.1)	52	22 212.87	(0.06)	-0.02	0.25	(0.05)
25	22 072.83	(0.06)	0.14	0.56	(0.10)	53	22 214.47	(0.06)	0.02	0.20	(0.05)
26	22 086.70	(0.06)	0.11	0.63	(0.15)	54	22 215.90	(0.06)	-0.01	0.26	(0.05)
27	22 099.01	(0.06)	0.05	0.49	(0.05)	55	22 217.24	(0.06)	-0.06	0.24	(0.05)
28	22 110.06	(0.04)	0.06	0.48	(0.06)	56	22 218.56	(0.04)	-0.05	0.22	(0.05)
29	22 119.93	(0.06)	0.03	0.35	(0.10)	57	22 219.84	(0.04)	-0.02	0.17	(0.05)
30	22 128.82	(0.06)	0.00	0.35	(0.03)	58	22 220.97	(0.06)	-0.07	0.24	(0.05)
31	22 136.89	(0.06)	0.01	0.32	(0.05)	59	22 222.16	(0.06)	0.00	0.17	(0.05)
32	22 144.16	(0.06)	-0.02	0.35	(0.05)	60	22 223.19	(0.04)	-0.03	0.25	(0.05)
33	22 150.78	(0.06)	-0.04	0.30	(0.03)	61	22 224.24	(0.04)	0.01	0.29	(0.05)
34	22 156.86	(0.06)	-0.02	0.40	(0.05)	62	22 225.18	(0.04)	-0.01	0.31	(0.05)
35	22 162.46	(0.06)	0.04	0.70	(0.05)	63	22 226.07	(0.04)	-0.04	0.20	(0.05)
36	22 167.52	(0.06)	0.02	0.42	(0.05)	64	22 226.98	(0.04)	-0.00	0.27	(0.05)
37	22 172.16	(0.04)	-0.01	0.29	(0.05)	65	22 227.81	(0.06)	-0.01	0.14	(0.10)
38	22 176.47	(0.06)	-0.00	0.30	(0.05)	66	22 228.63	(0.06)	0.02	0.30	(0.10)

rapidly with increasing n . For $11 \leq n \leq 30$ the width decreases from 2 to 3 cm^{-1} , to 0.35 cm^{-1} with an inverse power of n less than 3, which is the value known for atomic Rydberg states.⁴⁰ For all n levels above $n = 40$ a linewidth of $\approx 0.25 \text{ cm}^{-1}$ is found, while the laser linewidth is 0.08 cm^{-1} , as confirmed in simultaneous measurements of the Te_2 spectrum. This minimum linewidth was found not to be determined by laser intensity and possibly results from the ensemble of rotational states excited by the preparation laser.

Local maxima in the linewidth are seen around $n = 14, 22$, and possibly 35. These maxima correspond to a decrease in the intensity of the Rydberg transition and are thus most influenced by power broadening; in order to obtain acceptable signal to noise levels somewhat higher excitation laser pulse energies had to be used for these lines. An analysis of these local intensity dips and corresponding linewidth maxima will be given in a future publication.⁴¹

B. MATI measurements

In the MATI measurements a time delay of $6 \mu\text{s}$ between excitation and pulsed field ionization/extraction was found to yield the best balance between separation of prompt and delayed ions and retention of the ions in the collection region. Shorter ($4 \mu\text{s}$) and longer ($9 \mu\text{s}$) time delays resulted in no

significant differences in the overall form of the MATI spectra. Figure 5 shows the MATI-spectrum of DABCO taken with a bias field of 1.0 V/cm present during the excitation pulse, along with the position of the field-free IP determined by the Rydberg state progression, and the saddle-point energy E_{sp} given by $\text{IP} - 6\sqrt{\mathcal{E}} \text{ cm}^{-1}$ expected for ionization in a static electric field of $\mathcal{E} \text{ V/cm}$.^{10,37} According to classic theory, above the saddle point energy ($\text{IP} - 6 \text{ cm}^{-1}$ for Fig. 5) highly excited Rydberg states become unstable to ionization. The peak of the MATI spectrum lies at $n = 135$ with a FWHM of 6 cm^{-1} ($\Delta n = 60$). On the low-energy side of the MATI peak the Rydberg series is clearly seen (as in previous ZEKE studies²⁰) and is shown in more detail in the inset in Fig. 5. With the higher sensitivity of the present study a separate strong series of interloper peaks is observable, labeled $n' = 60 - 69$ in Fig. 5, which are displaced by a value of $\Delta\delta = 0.5$ from the np_{xy} series. This interloper series is not observed in the “total-ion” measurements described previously which are taken at zero-applied field. It is also seen in Fig. 5 that the signal extends to well above ($\approx 5 \text{ cm}^{-1}$) the field-free IP, while at the same time the disappearance of the signal at even higher frequencies is evidence for the blocking of prompt photo-ions in this MATI set-up.

MATI spectra taken at $0.5, 1.0, 2.0$, and 4.0 V/cm static

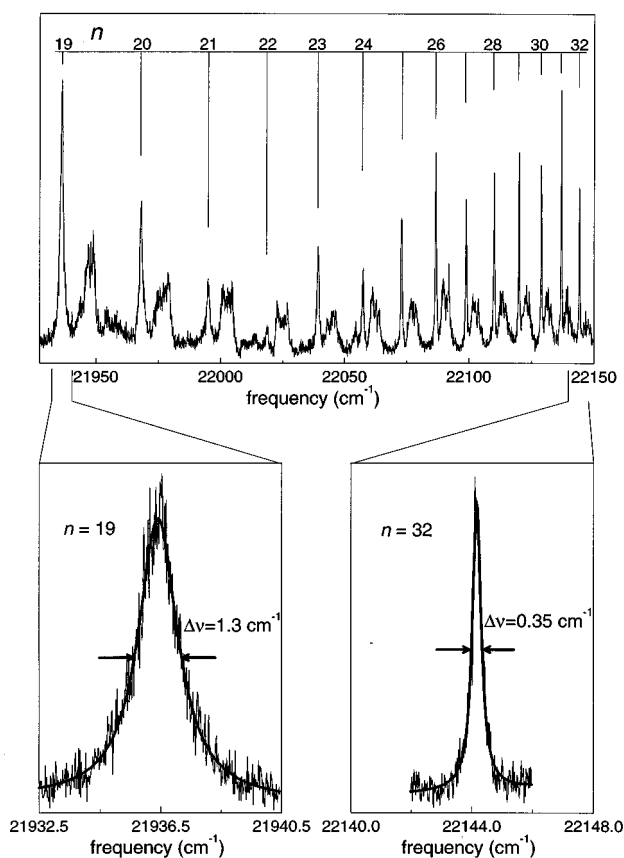


FIG. 3. Doubly-resonant excitation/vibrational autoionization spectrum of Rydberg levels in 1,4-diazabicyclo[2,2,2]octane (DABCO) after preparation of the ν_{24} mode in the S_1 state in zero applied electric field. After $4 \mu\text{s}$ the ions are extracted by a pulsed electric field and mass-selectively detected in a Wiley–McLaren set-up. The spectrum shows only a part of the measured Rydberg series. The lines are calibrated against the $^{130}\text{Te}_2$ absorption spectrum at 450°C , and fitted to a Lorentzian profile. This is shown in the lower part of the figure for $n=19$ and for $n=32$.

bias fields are shown in Fig. 6. In this series the reflector voltage (Fig. 2) is held constant, keeping the size of the collection region for ions formed by the delayed pulsed field ionization event constant. With increasingly larger bias fields the signal on the high-energy side decreases due to the lowering of the saddle-point energy. The position of the “interloper” series moves to lower energy as the bias field increases. Saddle point energies are indicated in Fig. 6, along with the positions of the high n values of the Rydberg series.

Pulsed field ionization/ion extraction in these MATI spectra occurs with a 200 V/cm step-pulse (Fig. 2). Assuming diabatic trajectories through the Stark manifold,^{9,10} n levels above $n=45$ ($\text{IP} - 4\sqrt{\mathcal{E}} = \text{IP} - 57 \text{ cm}^{-1}$) should be unstable to direct ionization. Levels with $n > 50$ have observable intensity in the MATI spectra shown in Figs. 5,6.

A MATI spectrum was also taken with a bias field of 1 V/cm applied shortly after the excitation laser pulse. Because the bias field could not thus far be applied in a proper fast-rising step the spectrum was not considered fully reliable and is not shown. Qualitatively, however, the signal taken with zero-applied bias field during the excitation pulse is signifi-

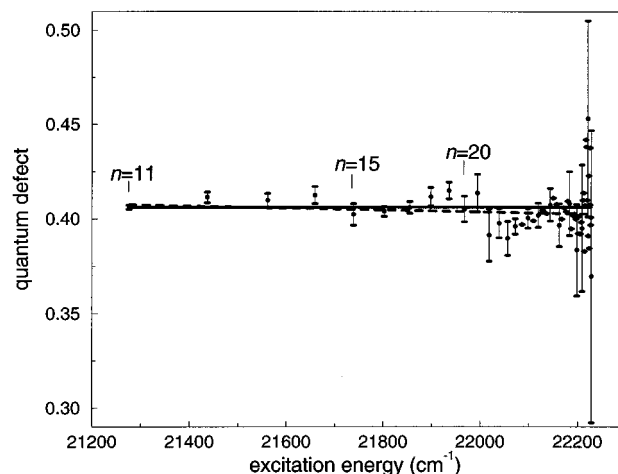


FIG. 4. The quantum defect δ of each Rydberg state as a function of the energy of the state, calculated from the observed line position where the fitted value of $22\,254.121 \text{ cm}^{-1}$ for the IP is used. Also shown in this figure are the (constant) quantum defect determined from the same fit (solid line), and the functional form of the n -dependent quantum defect $\delta_n = \delta + \epsilon R / (n - \delta)^2$, where ϵ represents a distortion parameter (dashed line).

cantly stronger than the static bias field signal, as also reported by Müller-Dethlefs and co-workers.³ Ito and co-workers¹⁵ have reported ZEKE spectra under these conditions using a 1 V/cm pulsed bias/extraction field. Their spectra, while of lower signal to noise than that of Fig. 5,

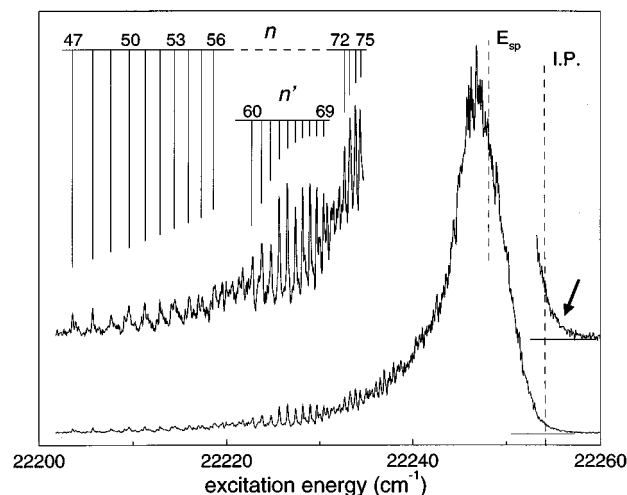


FIG. 5. Mass analyzed threshold ionization (MATI) spectrum of DABCO recorded in an electric bias field of 1.0 V/cm , after preparation of the ν_{24} mode in the S_1 state of DABCO. After $6 \mu\text{s}$ pulsed field ionization and extraction of the ions is performed with a pulsed field of 200 V/cm and the ions are mass-selectively detected in a Wiley–McLaren set-up. The voltage on the prompt ion reflector is set to 1720 V . The MATI peak comprises Rydberg levels in the $n=105\text{--}165$ part of the series. The upper trace shows an enlargement of a part of the same spectrum from which individual Rydberg lines clearly can be distinguished. Also indicated are the field-free IP determined by the Rydberg state progression, and the saddle-point energy $E_{\text{sp}} = \text{IP} - 6\sqrt{\mathcal{E}} [\text{V/cm}] \text{ cm}^{-1}$.

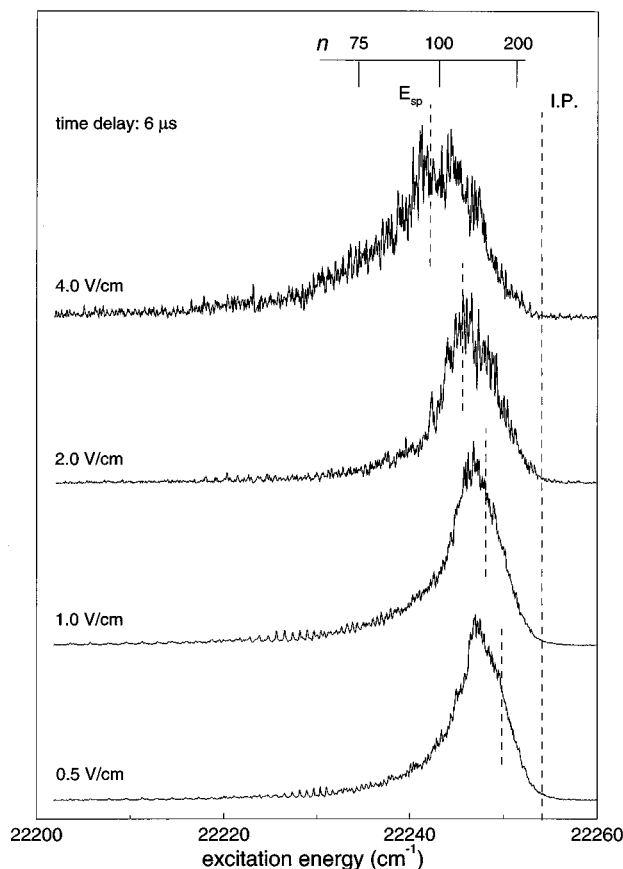


FIG. 6. MATI spectra of DABCO for four different values of the electric bias field in the excitation region. The spectra are all recorded with a delay of $6 \mu\text{s}$ between excitation of the Rydberg states and pulsed field extraction of the ions, and with a voltage of 1720 V on the prompt ion reflector. Also indicated are the field free IP determined by the Rydberg state progression, and the saddle-point energy $E_{\text{sp}} = \text{IP} - 6\sqrt{\mathcal{E}[\text{V/cm}]} \text{ cm}^{-1}$.

show that the highest Rydberg states contribute most to the signal compared to spectra obtained under static bias field conditions.

IV. DISCUSSION

A. Ionization potential, quantum defect, and linewidths

An ensemble of rotational states are prepared and probed in this study due to the 0.5 cm^{-1} bandwidth of the preparation laser. Owing to the effective rotational cooling [$T_{\text{rot}} < 2 \text{ K}$ (Ref. 28)] only states with $J, K < 5$ are present in the molecular beam. The $S_1 \ 24_0^1 \leftarrow S_0$ transition chosen has a FWHM of $\approx 1.5 \text{ cm}^{-1}$ (Ref. 28) which means that an (unknown) subset of these levels are excited by the narrower linewidth preparation laser. The IP thus reported reflects the zero-point vibrational energy of the ground electronic state and ion, the vibrational energy of ν_{24} in the ion [$\approx 1006 \text{ cm}^{-1}$ (Ref. 42)], and the selected rotational energy. Similarly, the δ value reflects the internal rovibrational energies.

In general, the coupling of rotational motion undergoes a transition from Hund's case (b) for the ground state molecule to Hund's case (d) for highly excited Rydberg states. Based

on studies in diatomics³⁹ this transition is likely complete by $n = 11$, the lowest Rydberg level accessible by vibrational autoionization in this study. In Hund's case (d) the Rydberg state energy for a diatomic is expressed by $T = T^{\text{ev}} + BN(N+1)$ with T^{ev} the rotationless term energy, B the rotational constant in the ion, and N the core rotational quantum number. Transitions in this limiting case follow $\Delta N = 0$.

For DABCO, a prolate symmetric top with $A = B \approx 2600 \text{ MHz}$ and $C \approx 3200 \text{ MHz}$ within 1% for all the involved electronic states (S_0, S_1, ion),⁴³ the selection rules and rotational profiles are more complicated since the excitation step starts from an e' vibration in the $3s \ (A_1')$ electronic state and ends in an $np_{xy} \ (E')$ electronic state with the same e' vibration excited ($\Delta v = 0$). Identifying the important components in the $e' \otimes e'$ final state is speculative and is best left to a later experiment where a single J, K state is prepared. In general, however, the rotational profile for transitions to the Rydberg states observed (Table I) should be very similar to direct transitions to the ion. Lorentzian line shapes were found to fit well for all the transitions measured, the center of each fit Lorentzian was taken as the transition energy. The IP obtained from the Rydberg formula fit thus also reflects the center or (weighted) average of the internal rotational energy excited. Significant differences between the reported IP and the rotationless IP are thus not expected.

Lorentzian profiles have been found to fit the lower ($n = 3 - 7$) Rydberg levels of benzene.⁴⁴ Rydberg state lifetimes obtained from these frequency domain measurements have also been confirmed for benzene by pump-probe femtosecond time-domain measurements.⁴⁵ For the lower n states of DABCO ($n < 30$) the linewidths measured (Table I) also reflect fast decay processes.²⁰ Above $n \approx 40$ a constant linewidth is measured, reflecting possibly the rotational transition profile of the ensemble of rotational states excited.

B. MATI measurements

Chupka has discussed the experimental and molecular characteristics necessary to obtain accurate high-resolution information from ZEKE/MATI measurements.⁷ In order to obtain an accurate IP, thus energy position of ionic energy levels, a sharp fall-off in the MATI/ZEKE signal is necessary, and at an energy position which is a predictable function of the applied electric field. For a MATI-type experiment with a static bias field the signal is expected to disappear at an energy $E = \text{IP} - 6\sqrt{\mathcal{E}(\text{V/cm})} \text{ cm}^{-1}$.⁷ Such behavior is strikingly demonstrated in a MATI-like study on H_3 ,³⁷ for example. For DABCO, under the present (and typical) experimental conditions this is not the case. Neither a sharp fall-off nor an obvious functional dependence of the MATI determined IP on the bias voltage is observed in Fig. 6. Furthermore it is seen in Figs. 5 and 6 that the signal extends to well above the field-free IP. While the absolute agreement between the MATI IP and the Rydberg extrapolated IP is quite satisfactory, the nonideal behavior of the DABCO MATI signal should most likely be considered as a result of the experimental design, and not necessarily as a

difference in large molecule versus small molecule dynamics.⁴ Even for the simple H₃ molecule estimation of ionization rates and especially laser polarization effects are complicated.³⁷ In the present experiment too little is known about the $e' \otimes e'$ transition measured, and the purity of the laser polarization is not controlled well enough (laser field is roughly parallel to Stark field) to expect ideal behavior. Still, the apparatus is quite typical for MATI experiments. The nonsystematics of the MATI signal indicates a simple correction of the measured MATI threshold for the applied electric field strength may be unreliable.

Considering the previous discussion of rotational contributions to the line shape it is possible that the above-IP signal is not simply due to the internal rotational energy. Theoretical studies^{46,35,47} have predicted a stabilization of excited neutral molecules to ionization due to core coupling effects, even for energies above the IP. When treated with quantum theory using parabolic coordinates³⁵ it has been shown that the electron can have an energy that is sufficient for ionization and still not ionize promptly. This could be an explanation for the appearance of the above threshold behavior of the MATI peak.

Interloper series such as those seen in Figs. 5 and 6 have been seen previously for other molecules.^{36–39} For Na₂ a similar appearing “stroboscopic” effect was observed³⁸ and ascribed to coupling of rotational motion to the Rydberg electron period. In DABCO the mix of rotational states and electric field dependence suggest a different mechanism. Electric field dependent interloper series have been observed in NO (Ref. 39) and ascribed to the appearance of an optically forbidden Rydberg series of another δ value which becomes allowed due to Stark mixing. Stark manifold mixing is also seen to result in shifting of the transition energy to positions halfway between the zero-field n values in H₂ (Ref. 36) and H₃.³⁷ Due to the similarity of the effect seen for DABCO and in the last two studies the manifold mixing (adiabatic noncrossing) mechanism seems more likely. More detailed studies are needed to confirm such an assignment.

“Normal” np_{xy} Rydberg states are also seen in the MATI spectra. While ionization of these states is energetically possible due to the 200 V/cm pulsed ionization field their presence is somewhat unusual in that such low n values ($n < 50$) have survived the 6 μ s delay. It is possible that such states survive in other molecules but do not appear so sharply as in the DABCO spectra.

V. CONCLUSIONS

Accurate measurements of the IP and quantum defect of Rydberg series of DABCO have been presented. The IP was determined from the np_{xy} series converging to $v = 1$ of the $\nu_{24}(e')$ mode in the molecular ion, which is the most conveniently prepared mode and the strongest, sharpest series in the molecule. The quantum defect for the np_{xy} series is also extracted. Fast decay processes are indicated by transition linewidths for $n < 30$. Above $n \approx 40$ a constant minimal linewidth is observed, most likely due to the rotational transition profile of the rotational ensemble excited. The IP observed in

the MATI spectra are in qualitative agreement with the Rydberg series IP but do not show sharp cut-off in signal above the saddle point energies. Interloper series are also observed as a function of applied electric fields. These show a very similar behaviour to Rydberg states of much smaller molecules, indicating the hydrogenlike nature of highly excited Rydberg states.

ACKNOWLEDGMENTS

This work is part of the research program of the “Stichting voor Fundamenteel Onderzoek der Materie (FOM),” which is financially supported by the “Nederlandse Organisatie voor Wetenschappelijk Onderzoek (NWO).” We thank also the Research Institute for Materials for support. U.E. thanks the James Franck program for Laser Matter Interaction.

- ¹K. Müller-Dethlefs and E. W. Schlag, *Annu. Rev. Phys. Chem.* **42**, 109 (1991).
- ²L. Zhu and P. Johnson, *J. Chem. Phys.* **94**, 5769 (1991).
- ³H. J. Dietrich, R. Linder, and K. Müller-Dethlefs, *J. Chem. Phys.* **101**, 3399 (1994).
- ⁴D. Bahatt, U. Even, and R. D. Levine, *J. Chem. Phys.* **98**, 1744 (1993).
- ⁵W. G. Scherzer, H. L. Selzle, E. W. Schlag, and R. D. Levine, *Phys. Rev. Lett.* **72**, 1435 (1994).
- ⁶G. B. Reiser, W. Habenicht, K. Müller-Dethlefs, and E. W. Schlag, *Chem. Phys. Lett.* **152**, 119 (1988).
- ⁷W. A. Chupka, *J. Chem. Phys.* **98**, 4520 (1993).
- ⁸E. Rabani, R. D. Levine, A. Mühlport, and U. Even, *J. Chem. Phys.* **102**, 1619 (1995).
- ⁹F. Merkt and R. N. Zare, *J. Chem. Phys.* **101**, 3495 (1994).
- ¹⁰H. A. Bethe and E. E. Salpeter, *Quantum Mechanics of One- and Two-Electron Atoms* (Plenum, New York, 1977).
- ¹¹W. L. Glab and J. P. Hessler, *Phys. Rev. A* **35**, 2102 (1987).
- ¹²C. Bordas, P. F. Brevet, M. Broeyer, J. Chevalere, P. Labsatu, and J. P. Perrot, *Phys. Rev. A* **60**, 917 (1988).
- ¹³C. R. Mahon, G. R. Janik, and T. F. Gallagher, *Phys. Rev. A* **41**, 3746 (1990).
- ¹⁴S. T. Pratt, *J. Chem. Phys.* **98**, 9241 (1993).
- ¹⁵M. Fujii, T. Ebata, N. Mikami, and M. Ito, *Chem. Phys. Lett.* **101**, 5780 (1983); *J. Phys. Chem.* **88**, 4265 (1984); M. Fujii, Y. Tsuchiya, and M. Ito, *ibid.* **92**, 2398 (1988); K. Tarazawa, M. Fujii, T. Ebata, and M. Ito, *Chem. Phys. Lett.* **189**, 592 (1992).
- ¹⁶M. Fujii, N. Mikami, and M. Ito, *Chem. Phys. Lett.* **99**, 193 (1985); M. Fujii, T. Kakinuma, N. Mikami, and M. Ito, *ibid.* **127**, 297 (1986); A. Goto, M. Fujii, and M. Ito, *J. Phys. Chem.* **91**, 2268 (1987).
- ¹⁷J. Hager, M. A. Smith, and S. C. Wallace, *J. Chem. Phys.* **84**, 6771 (1986).
- ¹⁸L. A. Chewler, M. Sander, K. Müller-Dethlefs, and E. W. Schlag, *J. Chem. Phys.* **86**, 4737 (1987).
- ¹⁹D. T. Cramb and S. C. Wallace, *J. Chem. Phys.* **101**, 6523 (1994).
- ²⁰U. Even, R. D. Levine, and R. Bersohn, *J. Phys. Chem.* **98**, 917 (1994).
- ²¹D. H. Parker and M. A. El-Sayed, *Chem. Phys.* **42**, 379 (1979).
- ²²G. J. Fisanick, T. S. Eichelberger, M. B. Robin, and N. A. Kuebler, *J. Phys. Chem.* **87**, 2240 (1983).
- ²³M. A. Smith, J. N. Hager, and J. C. Wallace, *J. Phys. Chem.* **88**, 2250 (1984).
- ²⁴J. H. Glowina, G. Arjavalingam, and P. P. Sorokin, *J. Chem. Phys.* **82**, 4086 (1985).
- ²⁵M. B. Robin, *Higher Excited States of Polyatomic Molecules* (Academic, New York, 1974, 1985).
- ²⁶X. Zhang, M. Smith, and J. L. Knee, *J. Chem. Phys.* **99**, 3133 (1993).
- ²⁷M. G. H. Boogaarts, P. C. Hinnen, and G. Meijer, *Chem. Phys. Lett.* **223**, 537 (1994); M. G. H. Boogaarts and G. Meijer, *J. Chem. Phys.* **103**, 5269 (1995).
- ²⁸D. Consalvo, M. Drabbels, G. Berden, W. L. Meerts, D. H. Parker, and J. Reuss, *Chem. Phys.* **174**, 267 (1993).
- ²⁹G. van den Hoek, D. Consalvo, D. H. Parker, and J. Reuss, *Z. Phys. D* **27**, 73 (1993).

- ³⁰J. Cariou and P. Luc, *Atlas du Spectre d'Absorption de la Molecule de Tellure* (CNRS, Paris, 1980).
- ³¹C. Jouvét, C. Dedonder-Lardeux, S. Martrenchard-Barra, and D. Solgadi, *Chem. Phys. Lett.* **198**, 419 (1992).
- ³²H. Krause and H. J. Neusser, *J. Chem. Phys.* **97**, 5923 (1992).
- ³³K. F. Willey, C. S. Yeh, and M. A. Duncan, *Chem. Phys. Lett.* **211**, 156 (1993).
- ³⁴H. Krause and H. J. Neusser, *Chem. Phys. Lett.* **213**, 603 (1993).
- ³⁵L. Ya. Baranov, R. Kris, R. D. Levine, and U. Even, *J. Chem. Phys.* **100**, 186 (1994).
- ³⁶E. Y. Xu, H. Helm, and R. Kachru, *Phys. Rev. Lett.* **59**, 1096 (1987).
- ³⁷C. Bordas and H. Helm, *J. Am. Phys. Soc.* **47**, 1209 (1992).
- ³⁸P. Labastie, M. C. Bordas, B. Tribollet, and M. Broyer, *Phys. Rev. Lett.* **52**, 1681 (1984).
- ³⁹S. Fredin, D. Gauyacq, M. Horani, C. Jungen, G. Lefevre, and F. Masnou-Seeuws, *Mol. Phys.* **60**, 825 (1987).
- ⁴⁰Hotop *et al.*, *Z. Phys. D, Atoms, Molecules and Clusters* **23**, 101 (1992).
- ⁴¹F. Remacle and R. Levine (work in progress).
- ⁴²According to Ref. 19 the ν_{24} vibrational energy is $\approx 5 \text{ cm}^{-1}$ lower in energy in the ion than in the ground state of the neutral. Using the measured energy of 1011.7 cm^{-1} (Ref. 28) this gives $\approx 1006 \text{ cm}^{-1}$ for the ion.
- ⁴³(Work in progress).
- ⁴⁴R. L. Whetten, S. G. Grubb, C. E. Otis, A. C. Albrecht, and E. R. Grant, *J. Chem. Phys.* **82**, 1115 (1985).
- ⁴⁵J. M. Wiesenfeld and B. I. Greene, *Phys. Rev. Lett.* **51**, 1745 (1983).
- ⁴⁶E. Lee, D. Farrelly, and T. Uzer, *Chem. Phys. Lett.* **231**, 241 (1994).
- ⁴⁷F. Remacle and R. D. Levine, *J. Chem. Phys.* (submitted).